ELSEVIER

Contents lists available at ScienceDirect

Chemical Geology

journal homepage: www.elsevier.com/locate/chemgeo





A bulk annealing and dissolution-based zircon concentration method for mafic rocks

A.L. Oliveira a,b,*, M.D. Schmitz , C.J. Wall , M.H.B.M. Hollanda b

- ^a Department of Geosciences, Boise State University, 1910 University Drive, Boise, ID 83725, USA
- ^b Instituto de Geociências, Universidade de São Paulo, Rua do Lago 562, São Paulo, SP 05508-080, Brazil

ARTICLE INFO

Editor: Dr Balz Kamber

Keywords: U—Pb geochronology Separation technique ZrSiO4

ABSTRACT

Zircon geochronology is applied to a variety of geological problems to precisely and accurately date rocks via U—Pb decay. Zircon is most abundant and easily recovered in intermediate to felsic rocks, including the silicic eruptives of bimodal large igneous provinces, or fractionated granophyres in mafic-ultramafic complexes. However, the concentration of zircon crystals by conventional density and magnetic separation methods is inefficient and/or ineffective for medium- to fine-grained mafic rocks, due to their rarity, small grain size, common association with ferromagnetic minerals, and/or occlusion by paramagnetic modal minerals. To address these shortcomings, we have developed and tested a zircon concentration method that is based on a combination of physical separation and chemical dissolution. The sample is initially ground to sand-size particles and heavy minerals concentrated via density on a water table. The heavy mineral-rich fraction is annealed by heating at 900 °C for 60 h, and then put through a series of acid digestions: aqua-regia, hydrofluoric acid, aqua-regia and finally hydrochloric acid. This new method allows the concentration of an almost pure zircon aliquot, since zircon is one of just a few minerals that can survive this bulk rock acid attack. The result is an efficient extraction of analytically viable amounts of zircon for U—Pb geochronology using tens of grams of rock sample, representing an increase up to a hundred times the recovery rates of conventional separation techniques for zircon concentration.

1. Introduction

The U-Pb decay system is a powerful and widely applied geochronometer due to the concentration of U and exclusion of initial Pb in common accessory minerals like zircon (ZrSiO₄) (Larsen Jr et al., 1952; Silver and Deutsch, 1963; Krogh, 1973; Ireland and Williams, 2003; Schaltegger et al., 2015). Additionally, the dual decay of ²³⁸U—²⁰⁶Pb and ²³⁵U—²⁰⁷Pb provides an internal cross-check of closed system behavior (Wetherill, 1956; Tilton et al., 1957), and the U isotopes have the most precisely determined decay constants among the commonly applied geochronological methods (Jaffey et al., 1971; Begemann et al., 2001). The development of the chemical abrasion method for mitigating open-system behavior in zircon, manifested as Pb-loss from U-rich, radiation-damaged domains (Mattinson, 2011; Mattinson, 2005), has solidified this mineral's ability to provide the most precise and accurate crystallization ages for igneous rocks. However, its use is not always applicable in mafic rock studies because basaltic magma emplacement temperatures and compositions are well outside of zircon saturation

conditions (Watson and Harrison, 1983; Harrison et al., 2007; Boehnke et al., 2013), and even in the more differentiated portions of doleritic to gabbroic mafic intrusions zircon crystals are commonly rare and small (Lee and Bachmann, 2014; Wall et al., 2018). The association of accessory phase nucleation with local silica saturation around ferromagnesian phenocrysts (Bacon, 1989) may also confound zircon concentrate using traditional magnetic separation.

U—Pb baddeleyite dating has had historical success for mafic rocks as this mineral can crystallize from the silica-undersaturated mafic melts that did not achieve widespread and/or prolonged zircon crystallization conditions. The earliest and most common applications of U—Pb baddeleyite geochronology were to Precambrian mafic intrusions (Krogh et al., 1987; LeCheminant and Heaman, 1989; Heaman et al., 1992), in geochronological contexts where ²⁰⁷Pb/²⁰⁶Pb or discordia upper intercept ages (to minimize age inaccuracy due to Pb-loss), with a resolution of several millions of years, were adequate to address the geological problems. Further application of U—Pb baddeleyite geochronology has been key to understanding ancient continental paleogeography, large

^{*} Corresponding author at: Department of Geosciences, Boise State University, 1910 University Drive, Boise, ID 83725, USA. E-mail address: ALISSON_OLIVEIRA@HOTMAIL.COM (A.L. Oliveira).

Table 1 Petrographic and compositional characteristics of the studied samples.

Sample	Rock		Mineralogy	Texture	Crystal size (mm)	SiO2 (%)	Al2O3 (%)	TiO2 (%)	MgO (%)	Fe2O3 (%)	CaO (%)	Na2O (%)	K2O (%)	Zr (ppm)	U (ppm)	CIPW norm	M value ¹
ST05- 03 ²	Leucogabbro	Plutonic	Plagioclase, pyroxene, quartz, alkali feldspar	Cummulatic	1.0–15.0	48.83	26.69		3.06	3.39	14.90			5.2	0.0245		
FC-1 ³	Anorthosite	Plutonic	Plagioclase, orthopyroxene, clinopyroxene, olivine	Cummulatic	2.0-7.0	49.43	25.31	1.38	2.11	4.34	12.71	3.24	0.42	65		Quartz- hypersthene	3.27
I	Basalt	Sub- volcanic	Plagioclase, pyroxene, magnetite, sulfides	Intergranular/ intersertal	0.5–1.5	51.30	12.96	3.40	3.96	14.54	7.33	2.90	1.82	287	1.0	Quartz- hypersthene	3.42
II	Basaltic andesite	Sub- volcanic	Plagioclase, pyroxene, magnetite, sulfides	Intergranular/ intersertal	0.5–1.5	52.60	12.69	2.90	3.69	13.39	6.25	3.62	2.27	352	1.2	Quartz- hypersthene	3.30
III	Basalt	Sub- volcanic	Plagioclase, pyroxene, magnetite, sulfides	Intergranular/ intersertal	0.5–1.5	No avai	lable geoch	emistry									
IV	Ol-basalt	Sub- volcanic	Plagioclase, olivine, pyroxene, magnetite, sulfides	Intergranular with olivine phenocrysts	1.0-4.0	50.50	14.82	1.97	7.33	11.42	8.31	3.65	0.76	100	0.5	Olivine- hypersthene	3.35
V	Basaltic andesite	Sub- volcanic	Plagioclase, pyroxene, magnetite, sulfides	Intergranular/ intersertal	0.5–1.5	53.24	16.27	1.26	3.46	11.42	8.94	3.22	1.24	204	0.9	Quartz- hypersthene	3.27
VI	Trachyandesite	Sub- volcanic	Plagioclase, quartz, magnetite, pyroxene, sulfides	Intergranular with plagioclase phenocrysts	0.2–3.5	57.30	13.30	2.23	2.51	11.8	5.16	3.45	3.19	520	1.8	Quartz- hypersthene	2.85

M = (Na + K + 2Ca)/(Al*Si) from Watson and Harrison (1983).
 From Fourny et al., 2016
 From Ibañes-Mejia and Tissot, 2019.

Chemical Geology 597 (2022) 120817

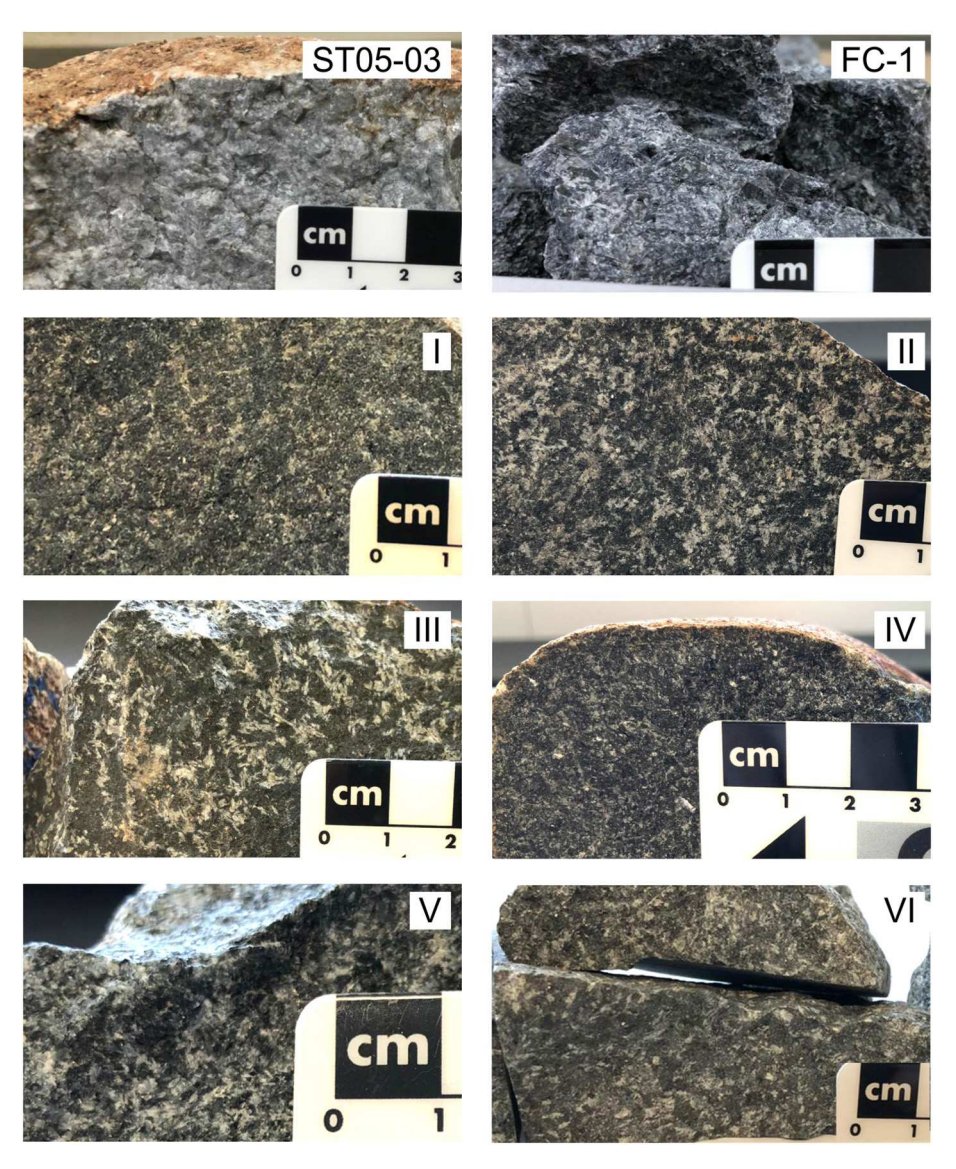


Fig. 1. Macroscopic aspects of the studied samples. Samples show the prevalence of plagioclase relative to the mafic minerals (except for sample IV).

igneous province (LIP) magmatism, and tectonic evolution (Heaman and LeCheminant, 2001; Heaman, 2009; Nilsson et al., 2010; Teixeira et al., 2015, 2019). U—Pb baddeleyite dating has been extended by in situ SIMS (Secondary Ionization Mass Spectrometry) dating of 'micro-baddeleyite' crystals within thin sections (Chamberlain et al., 2010), which would not normally be recovered during standard mineral separation, even with specialized techniques (Söderlund and Johansson, 2002). However, it is also increasingly recognized that baddeleyite is not as reliable for ²⁰⁶Pb/²³⁸U age-based geochronology because of secondary Pb-loss problems, since it cannot be treated by the chemical abrasion method (Rioux et al., 2010). This limitation hinders its use for highly accurate and precise (≤0.1% 2σ error) geochronology (Davis and Davis, 2010; Li et al., 2010; Schaltegger and Davies, 2017; Pohlner et al., 2020), particularly in Phanerozoic rocks where the ²⁰⁷Pb/²⁰⁶Pb chronometer has limited resolution.

With these recognized limitations of U—Pb baddeleyite geochronology, high-precision/high-accuracy U—Pb dating thus often relies on finding zircon crystals from differentiated felsic segregations within mafic intrusions. This approach applies a very selective filter to rocks and sampling sites, leaving many igneous events undated. Even so, recent works have been published on high-precision zircon U—Pb geochronology of LIPs in order to constrain global tectonic reconstructions (Bleeker and Ernst, 2006; Ernst et al., 2013) and to

correlate mafic large igneous events to mass extinctions and environmental changes (Davies et al., 2017; Heimdal et al., 2018; Schoene et al., 2019). It is the rarity and difficulty in concentrating zircon from mafic rocks that hinders our ability to extend these studies to other tectonomagmatic events. The dissolution method presented here follows upon decades of effort by the geochronological community to improve the techniques of U-Pb geochronology and expand their application to more challenging geological settings (Davis et al., 2003; Mattinson, 2011). The physical methods of separation of accessory minerals were detailed in the early work of Larsen Jr et al. (1952), and with the addition of water concentrating tables (Doe and Newell, 1965; Stewart, 1986) have been the mainstays of zircon extraction for geochronology. Neuerburg (1961) described a method for minor refractory mineral concentration using hydrofluoric acid digestion, with an emphasis on sulfide mineral purification. Concerns as to the effects of acid leaching on the geochemical and isotopic characteristics of minerals (Tilton, 1956; Silver and Deutsch, 1963; Todt and Büsch, 1981; Mattinson, 1994; Davis and Krogh, 2001) likely explain the lack of further developments in chemical separation techniques (two recent exceptions being the studies of Lawley and Selby, 2012 and Bea et al., 2018) until the breakthrough experiments of Mattinson (2005, 2011), who demonstrated the efficacy of high-temperature annealing of zircon prior to sequential acid dissolution for eliminating laboratory-induced elemental

Table 2Sample weights, in grams, for each preparation step.

Sample	Aliquot	Water tal	ole		Hand	$Frantz^1$		Heavy liq	uid ²	Anneal ³	Dissolved
		T1	T2	Т3	Magnet	Magnetic	Non-mag.	Heavy	Light		
ST05-03-A	547.1	117.3	141.8	126.9						Yes	85.70
ST05-03-B	625.0	113.2	152.8	168.4	6.88	41.1	64.99	6.31	58.68	Yes ⁴	6.06
FC1-A	1256.2	359.9	288.1	191.2						Yes	15.38
FC1-B	1199.7	268.2	236.1	272.0	51.61	193.4	23.9	1.05	22.85	No	none
I-A	789.7	112.4	189.3	262.8						Yes	112.4
I-B	936.4	164.3	241.2	261.7	39.75	119.2	3.72	0.01	3.71	Yes ⁴	8.41
II-A	1970.1	247.6	705.1	387.0						Yes	6.21
III-A	738.1	94.4	150.4	261.9						Yes	6.12
III-B	879.1	222.4	273.2	115.0	60.12	158.0	3.8	0.13	3.67	No	none
IV-A	2891.2	313.1	660.2	747.5						Yes	161.9
V-A	1194.3	278.8	344.9	216.0						Yes	22.59
VI-A	424.5	94.54	119.8	64.41						Yes	12.22
VI-B	456.7	175.5	113.4	29.51	65.48	107.6	2.38	0.25	2.13	Yes ⁴	8.13

- $^1~1.0~A$ magnet current, 7° forward slope (transport direction), 20° side tilt (settling direction).
- ² Methylene iodide (3.25 g/cm³).
- ³ 900 °C for 60 h; magnetic fractions only for B aliquots.
- ⁴ Only the magnectic fractions (from 'hand maget' and Frantz) were annealed and dissolved (see section 4.2 of the text).

and isotopic leaching effects and achieving concordant, closed-system U—Pb isotope systematics in treated zircon crystals. Over a decade of experience with modifications to the "chemical abrasion" method of Mattinson (2005, 2001), from single crystals of zircon (Macdonald et al., 2018; Isakson et al., 2022) to the isolation of zircon from traditional physical mineral separates of carbonatite (Stevens et al., 2013), led us to undertake a series of experiments that adapt physical separation, annealing, and chemical dissolution methodologies to successfully recover zircon from small mafic rock samples (< 1 kg).

2. Experimental procedures

2.1. Sample materials

The eight samples selected for experimental zircon recovery via chemical processing are intrusive mafic rocks of fine- to coarse-grain size. Two are coarse-grained gabbros from Precambrian mafic intrusions used as geochronological standards for U—Pb zircon dating; detailed information on the geology of these sites is found in Wall et al. (2016; leucogabbro ST05-03) and Paces and Miller (1993; anorthositic gabbro FC1). The other six samples are tholeitic diabase intrusions that are part of the Early Cretaceous Equatorial Atlantic Magmatic Province (EQUAMP) LIP in South America (Hollanda et al., 2019; Macêdo Filho and Hollanda, 2022). A summary of the main mineral assemblage and chemistry of these samples is given in Table 1, and their macroscopic aspects are seen in Fig. 1.

The standard sample ST05–03 comprises leucogabbro belonging to the Stillwater Complex Anorthosite zone II (Montana-USA) and dated to 2710.4 \pm 0.3 Ma (Wall et al., 2016). It is dominated by variably altered plagioclase (inferred original mode of $\sim\!80$ vol%) as randomly oriented, blocky, and strong polysynthetic twinned crystals ranging in size from 0.1 to 1.5 cm. The interstitial material consists mainly of large oikocrysts of inverted pigeonite (0.5 to 1.2 cm) with patchy actinolite-chlorite alteration. Small amounts of quartz ($\sim\!5$ vol%) occur with trace alkali feldspar in interstitial pockets between the plagioclase grains. The accessory minerals include zircon, titanite, rutile and baddeleyite associated with the "felsic" interstitial pockets of quartz and alkali feldspar.

The standard sample FC1 is an anorthositic gabbro of the Duluth Complex Anorthositic Series (Miller and Weiblen, 1990; Paces and Miller, 1993) dated to 1095.81 \pm 0.16 Ma (Swanson-Hysell et al., 2021). Sample FC1 is from an exposure of rock near Forest Center (Minnesota-USA) composed of cumulus plagioclase (85–95% mode) and minor olivine (poikilitic) with intercumulus orthopyroxene and clinopyroxene. There is some degree of alignment of plagioclase crystals that vary from medium to coarse ($\sim\!2$ to 7 mm). Late-stage minerals include inverted

pigeonite, hornblende, biotite, apatite, zircon, granophyre, and sulfides (Miller and Weiblen, 1990).

The petrographic aspects of the EQUAMP intrusions (labeled as samples I to VI) are similar; they are all nondeformed, fine- to medium-grained diabases dominated by Ca-plagioclase, two clinopyroxenes (augite >> pigeonite) and Fe—Ti minerals embedded in either intersertal or intergranular groundmass. In the hypocrystalline samples, devitrified glass can reach up to 10% by volume. In the holocrystalline samples, plagioclase is found as macro- (0.5 to 1 mm) and microcrystals (< 0.5 mm) very often exhibiting sub-ophitic to ophitic relationships with augite, especially evident in the holocrystalline samples. Sulfides and apatite are easily visible as accessory minerals. All samples are pristine, with loss of ignition values <1.3 wt%, although discrete post-magmatic alteration is denoted by sericitization in plagioclase. Samples I, II and VI are classified as high-Ti (TiO $_2$ > 2.2–3.4 wt%) basalt and basaltic andesites; samples IV and V are, respectively, an olivine basalt and an andesite with low-Ti (TiO $_2$ of 1.9 and 1.3 wt%) contents.

2.2. Starting preparation

Approximately 1–3 kg of each sample were processed by crushing and milling to pass through a 500 μm (35 mesh) sieve (see details in Table 2). In order to compare the efficiency of our chemical dissolution methodology with the conventional physical method, we divided the milled standards ST05–03 and FC1 and samples I, III and VI of the EQUAMP LIP into two roughly equal bulk aliquots using a Tyler-style splitter: 'A' for chemical dissolution and 'B' for conventional physical separation. The other three diabase samples (II, IV and V) were only prepared with the dissolution-based technique.

All sample aliquots were first wetted in ethyl alcohol and then loaded on a pyramid-style shaker table for water-based density separation, in a process similar to the one described by Söderlund and Johansson (2002). The wetted sample slurry was spooned onto the table in small aliquots of approximately 20 g each, and allowed to pass across the table; the groove and riffle design of the pyramid table very efficiently routes small, dense mineral grains across the table for concentration, as quantified by passing testing mixtures of quartz and pyrite (Stewart, 1986). Three table splits were individually collected, weighed, and labeled as T1, T2 and T3; T1 was the fraction containing the densest minerals and, therefore, prioritized for testing zircon recovery with both the chemical dissolution (fractions A/T1) and conventional physical (fractions B/T1) protocols.

Before dissolution, all fractions A/T1 were annealed in a muffle furnace at 900 $^{\circ}$ C for 60 h, in order to minimize the potential for leaching and fractionation of radiogenic Pb from its parent U in zircon

A.L. Oliveira et al. Chemical Geology 597 (2022) 120817

Table 3 Dissolution experiments.

Sample	Starting Wt.	Acid per	Sample/Reagent	Experimental	step ¹	Total	Final Wt.	Final W			
	(g) step (ml) (g/ml)		1	2	3	4	Hours	(g)	(%)		
First expe	rimental phase										
I-A				Oxide and sul	fide attack	Silicate	Phantom sili	cate attack			
				Stage one		attack	Stage three				
						Stage two					
1	5.01	5	0.401	HCl 6 M - 6	_	HF 29 M -	HCl 6 M -	HCl 6 M -	26.5	3.670	73.29
				h		15 h	2 h	0.5 h			
2	5.54	10	0.185	HCl 12 M -	-	HF 29 M -	HCl 6 M -	HCl 6 M -	27.5	1.485	26.79
				6 h		15 h	6 h	0.5 h			
3	10.05	20	0.201	HNO3 8 M -	_	HF 29 M -	HCl 6 M -	HCl 6 M -	23.5	0.708	7.05
				6 h		15 h	2 h	0.5 h			
4	10.31	20	0.172	HNO3 16 M	-	HF 29 M -	HCl 6 M -	HCl 6 M -	25.5	0.512	4.96
				- 6 h		15 h	4 h	0.5 h			
5	5.15	10	0.172	HCl 6 M - 2	HNO3 8 M -	HF 29 M -	AR dilute -	HCl 6 M -	23.5	0.477	9.27
				h	4 h	15 h	2 h	0.5 h			
6	5.06	20	0.084	HCl 6 M - 6	AR dilute -	HF 29 M -	AR dilute -	HCl 6 M -	38.5	0.317	6.27
				h	15 h	15 h	2 h	0.5 h			
7	5.17	10	0.148	HCl 12 M -	AR dilute -	HF 29 M -	HCl 6 M -	HCl 6 M -	27.5	0.190	3.68
				2 h	4 h	15 h	6 h	0.5 h			
8	10.06	20	0.144	HCl 12 M -	AR dilute -	HF 29 M -	AR dilute -	HCl 6 M -	46	0.107	1.07
				6 h	15 h	18 h	6 h	1.0 h			
9	10.27	20	0.147	HCl 12 M -	AR dilute -	HF 29 M -	AR dilute -	HCl 6 M -	46	0.209	2.03
				6 h	15 h	18 h	6 h	1.0 h			
10	10.19	20	0.204	AR dilute -	_	HF 29 M -	AR dilute -	HCl 6 M -	40.5	0.835	8.19
				18 h		18 h	4 h	0.5 h			
11	5.02	16	0.129	AR dilute -	_	HF 29 M -	HCl 6 M -	HCl 6 M -	23.5	0.281	5.60
				6 h		15 h	2 h	0.5 h			
12	5.18	20	0.104	AR dilute -	_	HF 29 M -	AR dilute -	HCl 6 M -	40.5	0.166	3.20
	0.10	20	0.101	18 h		18 h	4 h	0.5 h	1010	0.100	0.20
13	5.07	24	0.090	AR dilute -	_	HF 29 M -	AR dilute -	HCl 6 M -	53	0.147	2.91
	0.07		0.030	24 h		24 h	4 h	1.0 h	00	011 17	2.71
Cocond Ex		_									
	perimental Phase	е		Ctoro ono		Ctaga trus	Ctooo thuo				
I-A	0.00	20	0.005	Stage one		Stage two	Stage three	11011014	F0	0.010	0.407
14	2.03	20	0.025	AR - 24 h	_	HF 29 M -	AR - 4 h	HCl 12 M -	53	0.010	0.487
						24 h		1.0 h			
15	4.04	20	0.050	AR - 24 h	-	HF 29 M -	AR - 4 h	HCl 12 M -	53	0.033	0.826
						24 h		1.0 h			
16	6.04	20	0.075	AR - 24 h	_	HF 29 M -	AR - 4 h	HCl 12 M -	53	0.212	3.51
						24 h		1.0 h			
17	8.16	20	0.102	AR - 24 h	-	HF 29 M -	AR - 4 h	HCl 12 M -	53	0.246	3.01
						24 h		1.0 h			
ST05-											
03-A											
1	2.57	20	0.032	AR - 24 h	-	HF 29 M -	AR - 4 h	HCl 12 M -	53	0.0016	0.064
						24 h		1.0 h			
2	5.05	20	0.063	AR - 24 h	-	HF 29 M -	AR - 4 h	HCl 12 M -	53	0.0010	0.021
						24 h		1.0 h			
3	10.05	20	0.126	AR - 24 h	_	HF 29 M -	AR - 4 h	HCl 12 M -	53	0.0856	0.852
						24 h		1.0 h			
4	20.06	20	0.251	AR - 24 h	_	HF 29 M -	AR - 4 h	HCl 12 M -	53	13.777	68.7
						24 h		1.0 h			
VI-A											
1	2.13	20	0.027	AR - 24 h	-	HF 29 M -	AR - 4 h	HCl 12 M -	53	0.0001	0.003
						24 h		1.0 h			
2	4.05	20	0.051	AR - 24 h	_	HF 29 M -	AR - 4 h	HCl 12 M -	53	0.0003	0.008
2						24 h		1.0 h			
2											
3	6.04	20	0.075	AR - 24 h	_	HF 29 M -	AR - 4 h	HCl 12 M -	53	0.1097	1.82

 $^{^{1}}$ AR (aqua-regia) = 1:3 16 M HNO $_{3}$ to 12 M HCl; AR dilute = 1:1 aqua regia to H $_{2}$ O.

crystals during laboratory dissolution (e.g., Mattinson, 2005, 2011). Weighing of the (1) initial bulk samples, (2) the fractions Tn, (3) the fraction A/T1 after annealing, and (4) the fractions B/T1 after magnetic and heavy liquid separation was done in a PM3002-S/FACT Mettler Toledo balance.

2.3. Conventional (physical) separation protocol

All B/T1 fractions were first exposed to a plunger-type hand magnet

in order to remove ferromagnetic materials including magnetite as well as iron filings from the milling process. The magnetic material weights were recorded and these 'hand magnet' fractions were stored for subsequent experiments. The non-ferromagnetic B/T1 fractions were then run through a Frantz Isodynamic Magnetic Separator at 1.0 A current to the electromagnet, 7° forward slope (along the transport direction), and 20° side tilt (for gravitational sorting). The non-paramagnetic B/T1 fractions were immersed in methylene iodide (specific gravity of 3.25 g/cm³) in a glass separatory funnel to separate high- from low-density

² Step 5 immersed in ultrasonic bath.

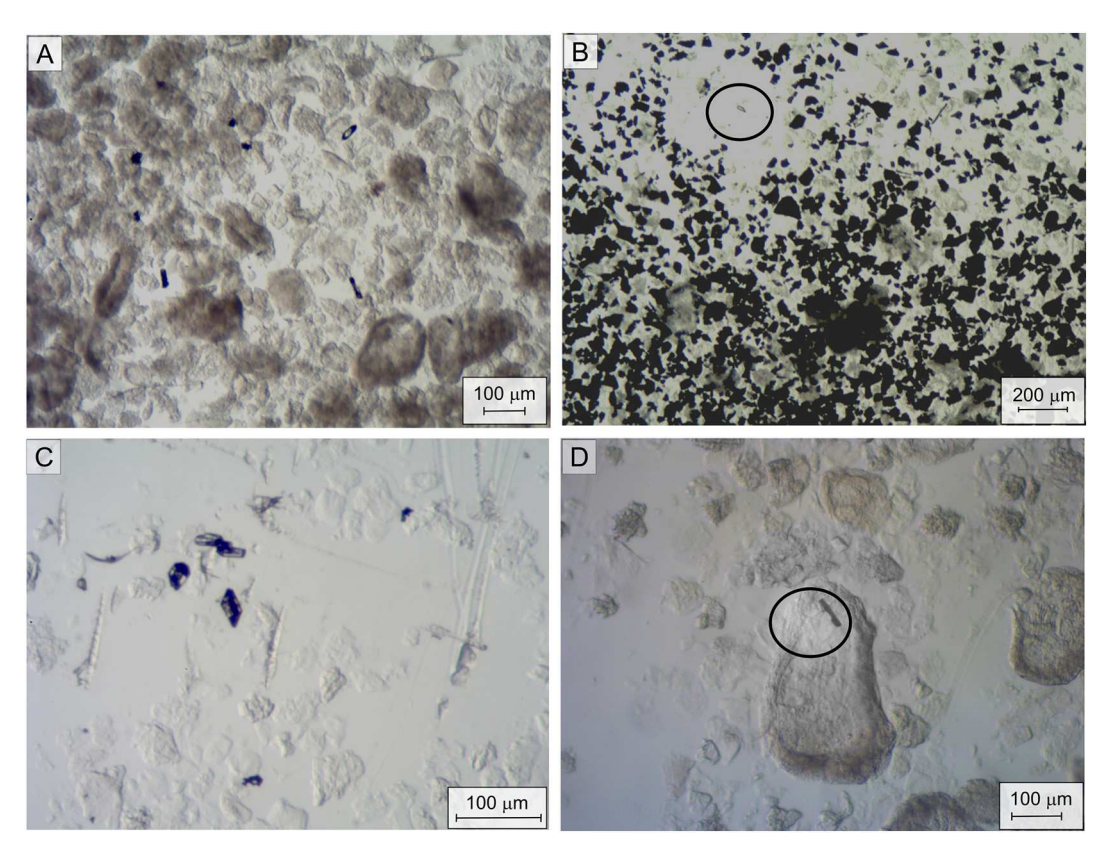


Fig. 2. Mineral concentrates from dissolution beakers 12 (A), 8 (B), 13 (C) of sample I-A and from a combined magnetic aliquot dissolved from sample VI-B (D). A – Phantom silicates (see text for definition of the term) and three zircon crystals, other undissolved oxides are also present. B – Phantom silicates and oxides that failed to dissolve, note one zircon crystal (black circle). C – Zircon crystals concentrated from the best chemical dissolution from the first experimental phase, many phantom silicates and a few oxides failed to dissolve, but the overall result was promising and instructive for the second experimental phase. D – Zircon included on a phantom silicate crystal (black circle).

minerals. Heavy liquids and grains were emulsified by repeated stirring in order to promote settling of small and dense grains. After >15 min of repeated agitation and settling, heavy minerals were tapped from the bottom of the funnel and rinsed thoroughly with acetone, dried, and removed to a polystyrene petri dish for grain examination and counting.

2.4. Chemical separation experiments

All chemical dissolution experiments were carried out in a vertical laminar flow workstation (Microzone) purged with ULPA-filtered (Class 10) air and performed in 60 ml Savillex® PFA beakers using reagent (ACS) grade acids (hydrofluoric, hydrochloric and nitric), either concentrated or diluted 1:1 with deionized water. The beakers were placed on a hot plate at 150 °C for all dissolution steps. The starting amount of material used in each step was weighed on a high-precision balance (AB265-A Mettler Toledo). Detailed information for each experimental aliquot is provided in Table 3. After each experimental step, the supernatant solutions were decanted with a pipet under a microscope and the residues rinsed with Milli-Q water before the addition of the next acid step. Importantly, at no time during the acid treatment steps were the solutions taken to dryness, thus avoiding the formation of insoluble fluorides. Final rinsed sample residues were dried, weighed, and removed to a polystyrene petri dish for grain examination and counting. Quantification of zircon from samples was done using a Leica M80 microscope coupled with a Leica MZ170HD camera. The ImageJ software package (National Institutes of Health, https://imagej.nih.gov) was used to quantify zircon crystals from two samples (ST05-03-A and FC1-A), and the other samples were measured by manually counting the zircon crystals. Individual frames of photoimagery of the ST05-03-A and FC1-A separates were also manually counted to check the

reproducibility of the ImageJ counting.

2.5. Mass spectrometry

Following chemical dissolution, recovered crystals were mounted on double-sided tape (Kapton #PPTDE-1½, double-sided polyamide) for surface compositional and isotopic analysis by laser ablation inductively coupled plasma mass spectrometry (LA-ICPMS) using a New Wave Research UP-213 Nd:YAG UV (213) laser ablation system coupled to a ThermoElectron X-Series II quadrupole mass spectrometer, following methods described in Macdonald et al. (2018). To assess the integrity of the chemical dissolution process for retaining closed system isotopic behavior, single crystals of zircon from sample FC1-A were analyzed for their U—Pb isotope ratios by the CA-IDTIMS method (Mattinson, 2005) according to the methods detailed in Macdonald et al. (2018) and Swanson-Hysell et al. (2021).

3. Results

3.1. Evaluation of the efficiency of reagents and duration of bulk rock dissolution

In a first set of experiments, we evaluated: (1) the amount and concentration of acids needed to efficiently dissolve the minerals, and (2) the optimal time required for complete dissolution. These parameters were tested using the fraction T1 of sample I-A (see Table 3), taken as representative of a typical fine-grained quartz-normative tholeiitic dolerite. We split the post-annealed fraction A/T1 into thirteen aliquots for testing; weights varied between 5 and 10 g of material, while the volume of acid per dissolution step was varied from 5 to 24 ml. Each

Table 4Zircon yields from chemical dissolution vs conventional separation.

Sample	Processed sample (g) ¹	# of zircon crystals recovered	# zircon crystals / g	zircon sizes (µm)
Chemical	dissolution			
ST05-	85.70	760^{2}	8.9	<50-300
03-A				
FC1-A	15.38	336^{2}	21.8	100-1500
I-A	112.35	53	0.47	<120
II-A	10.37	4	0.39	<120
III-A	10.24	5	0.49	<120
IV-A	211.88	13	0.06	<120
V-A	22.59	22	0.97	<120
VI-A	12.22	451	36.9	50-200
Convention	onal separation			
ST05-	113.24	67	0.59	>150
03-B				
FC-1-B	268.91	392 (33 ³)	1.46	150-1500
I-B	164.29	0	0.00	_
III-B	222.39	6	0.03	<120
VI-B	175.45	5	0.03	100-250

¹ Mass of sample processed by chemical dissolution or physical separations (heavy liquids and magnetic separation).

experiment was designed around three *stages* of dissolution and proceeded in four or five *steps* (stage 1 – steps 1 and 2, stage 2 – step 3, stage 3 – steps 4 and 5). The first stage was aimed at the dissolution of oxide and sulfide minerals in one or two steps via hydrochloric and nitric acids, or their mixture as dilute aqua regia. The second stage was focused on a single step breakdown of silicate bonds in hydrofluoric acid (Neuerburg, 1961). The third stage targeted in two steps the dissolution and removal of the residues after treatment with hydrofluoric acid, using first aqua regia or hydrochloric acid, and then hydrochloric acid with ultrasonification. The success of modifications to each experimental stage was assessed by the residual weight of sample after the entire process.

The first batch of aliquots treated the problem of how to eliminate Fe—Ti oxides and sulfides prior to the silicate minerals, two experiments were performed with HCl only (concentrated, 12 M, and diluted 1:1, 6 M), and two with HNO $_3$ only (concentrated, 16 M, and diluted 1:1, 8 M). These four experiments also varied the starting sample amounts and sample:acid ratios. From the results, we found that the combination of smaller sample:acid ratios (\sim 0.2 g/ml) and use of HNO $_3$ (beaker 5) resulted in greater dissolution efficiency for the same second and third stage treatments and procedure times (24–27 h). The weight of the remaining material was drastically reduced from 73% and 26% for HCl only versus 7% and 5% for the HNO $_3$ -based stage one dissolutions. Subsidiary controls on dissolution efficiency were the acid strength (concentrated versus 1:1 diluted) and sample:acid ratios (0.4 versus 0.2 g/ml).

In a second set of aliquots, we modified the experimental protocol to incorporate sequential HCl and HNO $_3$ or aqua regia steps in both stage one and stage three and varied the amount of time of total acid reaction between 23.5 and 46 h. We found the greatest efficiency of dissolution in these experiments resulted from the longest times of reaction, with those lasting 46 h reducing the sample quantities to between 1 and 2% of the starting weight, compared to from 9 to 4% for durations of 23.5 to 38.5 h.

The third and final set of aliquots of the first experimental phase simplified stage one to a single dilute aqua regia reaction step of varying duration. Stage two and three durations were also varied by total duration, from 23.5 to 53 h. While three aliquots had a consistent sample:acid ratio of 0.09 to 0.13 g/ml, one aliquot was set at 0.20 g/ml; this aliquot, like others in prior sets with higher sample:acid ratios, was the least efficiently dissolved, indicating a solubility limit for the dilute

acids (excepting HF) used in the first experimental phase. Also, like early sets, greater dissolution efficiency was confirmed for longer durations of the entire procedure (46 to 53 h).

Observations via optical microscopy of the most efficiently dissolved aliquots showed that beaker 12 (3.2% residue) had many partially dissolved silicate crystals (here referred as "phantom" silicate crystals, Fig. 2A) and a few oxides/sulfides. These phantom crystals are the residual frameworks of silicate minerals that were attacked by the 29 M HF but failed to be dissolved on the subsequent steps of aqua-regia and HCl (Table 3). Conversely to beaker 12, beaker 8 had many oxides and sulfides that failed to dissolve, and just a few phantom silicates (Fig. 2B). The undissolved minerals from beaker 8 made it difficult to pick because the high relief and opacity of the oxides hindered the ability to easily locate zircon crystals.

Beaker 13 was the most successfully dissolved aliquot from the first experimental phase. It still had many undissolved phantom silicate crystals but almost all non-silicates were dissolved, which made it possible to find zircon crystals even by using a small (5 g) initial mass (Fig. 2C). In this dissolution routine, the main mass losses were observed after the first aqua regia step (most oxides and sulfides dissolved) and after the last step of all, the ultrasonic bath using HCl (where the phantom silicates were dissolved). This aliquot demonstrates that the first dissolution of oxides and sulfides in aqua regia is of a major importance and is optimized by a longer (24 h) dissolution. The same is true of the post-HF reaction dissolution by multiple, longer duration aqua regia (4 h) and HCl (1 h) steps to dissolve the phantom silicates.

3.2. Evaluation of sample: acid proportions for optimal dissolution

Having established the importance of aqua regia for first stage dissolution of oxides and sulfides, and treatment durations of second and third stage dissolutions, these factors were maximized by the use of concentrated acids and longer reaction times (Table 3). The goal of the second experimental phase was to optimize the sample-to-reagent ratio by maintaining the best experiment routine (using a concentrated version of the reagents) and varying the amount of initial sample to see if the refractory phases would completely dissolve. Additionally, it was also used to look for the sample-to-reagent saturation limit of this technique for sample I-A, as a proxy for tholeitic mafic compositions. Furthermore, samples ST05–03-A and VI-A were used to check if this routine would also effectively dissolve different rock types in terms of geochemistry, texture, and crystal sizes.

For diabase sample I-A, the starting weights ranged from 2 to 8 g. For sample VI-A, we used three aliquots of 2, 4 and 6 g, whereas four aliquots of ST05–03-A (2.5, 5, 10 and 20 g) were treated. All aliquots were exposed to 20 ml of acid per experimental step, and constant treatment durations. For all three samples, a clear solubility limit was presented in sample quantities greater than 5 g, with residual sample percentages increasing by a factor of 4, 40, and 200 for samples I-A, ST05–03-A, and VI-A, respectively. For sequential 20 ml aliquots of acid, the maximum effectively dissolved sample quantity is approximately 4 g.

Microscopic observations from the second experimental phase were also instructive: on beaker 14 (2 g of sample I-A) there were 10 zircon crystals found and phantom silicates were present on a very low proportion. For beaker 15 (4 g) more than 20 zircon crystals were found but some phantom silicate crystals were left, which made the picking processes somewhat difficult. On beaker 16 (6 g) there were many phantom crystals and the amount of non-zircon phases including undissolved oxides made it difficult to spot a zircon. Lastly, beaker 17 (8 g) had many undissolved silicates and oxide/sulfide crystals.

Samples ST05–03-A and VI-A were, by contrast to sample I-A, relatively easily dissolved. Beaker 1 from sample ST05–03-A (2.5 g) had more than 30 zircon crystals and no refractory phases, while beaker 2 (5 g) had, correspondingly, more than 60 crystals in a pure zircon concentrate. Beakers 3 and 4 were used mainly to test how far we could push the sample-to-reagent ratio, but the results showed that the

² Count using ImageJ software on photomicrographs.

³ Baddeleyite crystals.

A.L. Oliveira et al. Chemical Geology 597 (2022) 120817

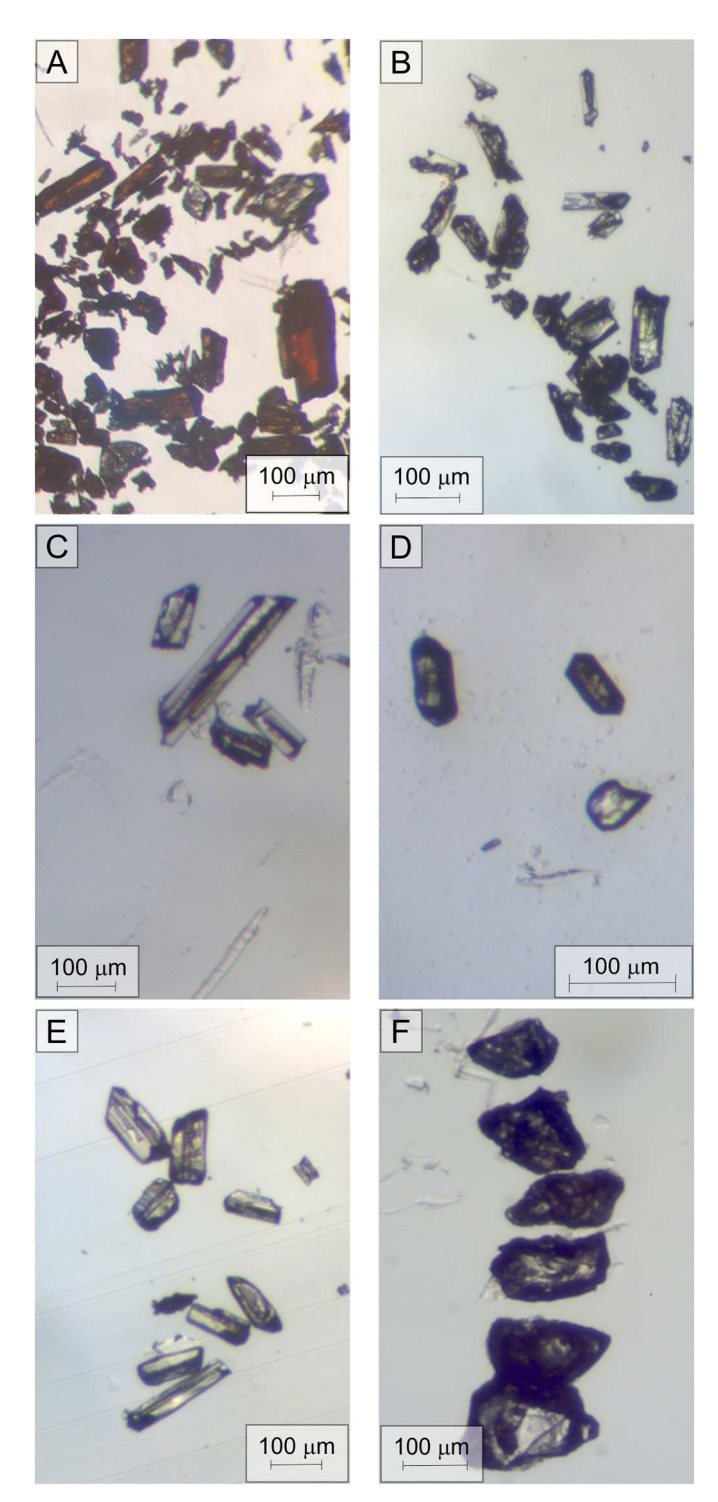


Fig. 3. Zircon concentrates obtained by the chemical dissolution method. A – Sample ST05–03-A, prismatic crystals with a brownish color and sizes that vary from <50 to 300 μm . B – Zircon crystals from sample I-A, prismatic euedral thin crystals with melt channels. C – Sample V, elongated and prismatic thin crystals with widespread melt channels. D – Zircon from sample IV-A, a small number of zircons recovered from an olivine-bearing rock. Crystals were prismatic to slightly anedral and smaller than 80 μm . E – Zircon crystals from the chemical dissolution of sample VI-A, blocky to elongated crystals range up to 200 μm in size, encompassing melt channels like the zircons from the other mafic tholeitic dikes. F – Mg-Spinels, a common refractory phase from the bulk dissolution of most mafic dikes.

solution saturated somewhere between 5 and 10 g, so both aliquots failed to dissolve efficiently. In fact, beaker 4 dissolved less than 35%, reiterating once more that the saturation limit does not follow a linear relation with the sample-to-reagent ratio. A similar dissolution was also observed for sample VI-A, where beakers 1 and 2 dissolved almost the entire sample (a few oxides survived), but once the saturation was achieved the sample stopped dissolving. Thus, an increase of 50% in initial mass from beaker 2 to 3 resulted on approximately 300 times more sample after all dissolution steps. Interestingly, a somewhat considerable number of oxides survived the dissolution steps on this sample, while no phantom silicates were left, which points toward the exhaustion of the aqua regia in stage one as a limit on dissolution efficiency.

3.3. Crystals obtained by the conventional versus chemical separation methods

Samples ST05-03-B, FC1-B, I-B, III-B and VI-B were prepared by the conventional separation routine and the number of zircon crystals recovered was summarized on Table 4. The two standards were treated to confirm that our separation routine was efficiently recovering zircon, while dike samples I—B, III-B and VI-B were used to test the recovery efficiency for fine- to medium-grained mafic (basalt) to intermediate (andesite) rocks. These results were compared to the chemical dissolution (A aliquots) recovery for each of those samples (Table 4). The resulting zircon yields show that the conventional routine is less efficient than the chemical dissolution technique proposed here. Expressed as # zircon crystals per gram of T1 (post-water table) sample processed, the chemical dissolution yield ranged from 0.06 to 0.97 for the diabase samples versus 0 to 0.03 when they were treated by the standard physical separation. For the most part, zircon crystals obtained from the conventional physical separation routine were larger in evolved samples (ST05-03, FC-1 and VI) and fewer on mafic dikes, although no difference in habits, colors or inclusions were noted between the two methods.

Overall, standard samples ST05–03-B and FC1-B yielded dozens to hundreds of zircons by the conventional separation (Table 4) that, in general, were larger than 150 μ m in longest diameter. From the ST05–03-B sample, zircon crystal recovery per sample mass prepared was about 0.59 crystals per gram, while for the FC1-B anorthosite this number was as high as 1.46 crystals per gram. Contrary to the standards, diabase samples III-B and VI-B had a low recovery rate of zircon crystals (\leq 0.03 crystals per gram), and no zircon was found in sample I—B. Of all of the samples examined, only aliquot FC1-B contained baddeleyite (33 crystals, or 0.12 crystals per gram).

Zircon crystals separated from sample ST05–03-A using chemical dissolution were colorless, varied from $<\!50~\mu m$ to $500~\mu m$ (Fig. 3A), had mainly anhedral habits, and the final concentrate had 760 crystals counted by the ImageJ software, or 8.9 crystals per gram of sample (Table 4). Zircon was accompanied by rutile in a ratio of $\sim\!1:\!30$, but this mineral was readily distinguished by its elongate prismatic habit and reddish-brown color. Also, the dissolution of sample ST05–03-A was done using a last step on the ultrasonic cleaner, which could induce minor breakage of some bigger crystals into smaller pieces (thus increasing the number of crystal fragments counted) but is unlikely to be solely responsible for the greater than tenfold recovery efficiency of the chemical dissolution method (Table 4).

Zircons from sample FC1-A were anhedral to prismatic, colorless, flattened and ranging up to 1.5 mm in longest dimension of thin prismatic crystals. Anhedral crystals were blocky and, for the most part, crack-free. Approximately 330 crystals were recovered from dissolving a little more than 15 g, yielding 21.8 zircon crystals per gram, again a greater than tenfold improvement over the conventional aliquot FC1-B (Table 4).

Diabase (dike) samples I-A (Fig. 3B), II-A, III-A and V-A (Fig. 3C) all yielded zircon after bulk dissolution (Table 4). Crystals from these

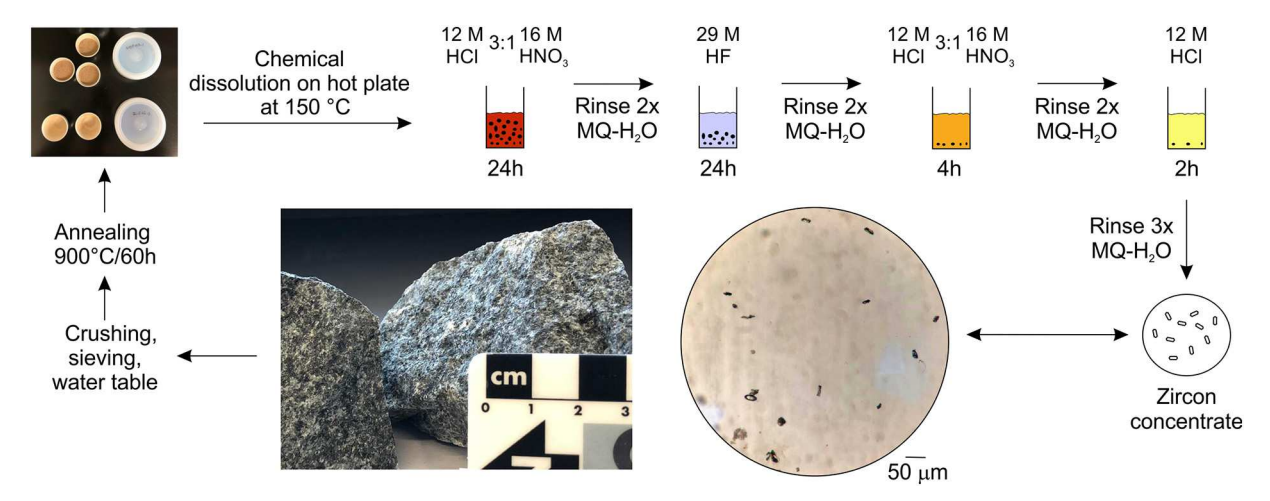


Fig. 4. Schematic flowchart for the chemical dissolution method, from a whole-rock sample to a concentrated zircon aliquot.

samples were $<120~\mu m$, had prismatic to skeletal habits and melt channel inclusions, all fast-cooling characteristics. Sample IV-A (Fig. 3D) was by far the most difficult to concentrate; the presence of olivine is indicative that this rock did not achieve widespread zircon saturation conditions (melt undersaturated in SiO₂). On the first 20 g dissolved, we did not concentrate any zircon crystals, and the dissolution residue provided the greatest amount of phantom silicate crystals from any sample processed. As expected, more acid volume was required to efficiently digest minerals in this more mafic rock compositions, and this was the only sample that was treated by the dissolution routine with a sample:acid ratio smaller than 0.10 g/ml. The final result was 13 zircon crystals concentrated after dissolving more than 200 g of sample, e.g., the least amount of zircon per dissolved sample (Table 4). Additionally, zircon crystals from this sample were not elongated and did not have melt channels as observed in every other dike sample. Lastly, sample VI-A was collected from an andesite dike and was the most evolved diabase in composition in terms of SiO2 and Zr. By the dissolution of just a few grams of sample we were able to recover a substantial number of crystals (Fig. 3E; Table 4), a contrasting finding when compared to the low recovery obtained from the conventional separation (Table 4). Prismatic to skeletal habits and melt channel inclusions were characteristics of these crystals, as were slightly larger sizes (up to $200 \mu m$) compared to the more mafic diabases.

3.4. Mineralogy, geochemistry, and age characterization

The refractory residues recovered from diabase samples I-A, IV-A, V-A and VI-A were investigated by LA-ICPMS for a rapid reconnaissance of their mineralogy, and the trace element geochemistry and U—Pb dates of the recovered zircon. The complete data set is housed in Supplementary Table 1. In addition to zircon, red-brown prismatic rutile was an abundant refractory mineral in sample ST05–03-A as confirmed by LA-ICPMS spectral scanning semiquantitative analysis. A further refractory phase was consistently found in small quantities in all diabase residues of the chemical dissolution method, and was identified as a Mg-spinel (Fig. 3F) by LA-ICPMS spectral scanning semiquantitative analysis. The presence of such minerals could not be avoided because the acid attacks regularly failed to dissolve them in all experiments. However, these crystals were blocky, anhedral to slightly tabular shaped, bigger than most zircon crystals (up to 250 μ m), transparent to light gray colored, and markedly more fragile than zircon.

Except for the olivine basalt (sample IV-A), most zircon crystals recovered from the EQUAMP samples that were investigated by quantitative standardized LA-ICPMS provided Cretaceous U—Pb dates (Supplementary Table 1) and are considered as primary magmatic phenocrysts, since EQUAMP rocks are prevalently intruded in the

Valanginian Stage (Hollanda et al., 2019; Oliveira et al., 2021). These zircon phenocrysts display REE patterns characteristic of highly evolved igneous compositions (Fig. 5), with pronounced negative Eu anomaly (Eu/Eu* = 0.03–0.34; av. 0.09), positive Ce anomaly, a slight enrichment in heavy REE compared to light REE (Lu_N/Sm_N = 0.84–114.45; av. 28.7), and \sum REE as high as 17,700 ppm. Th and U contents range up to 14,000 ppm and 3000 ppm, respectively, with Th/U ratios mostly >1.0 and up to 4.7, typical of mafic starting liquids.

Xenocrystic zircon is predominant in sample IV-A, and less abundant in the other diabases. These crystals provided Precambrian ages ranging from 485 to 2200 Ma (Supplementary Table 1), which are herein assumed to be inherited from the regional basement rocks that host the EQUAMP dikes. Overall, they are also distinguished geochemically from phenocrystic zircon by their small positive to negative Ce and Eu anomalies, a more pronounced enrichment in heavy REE compared to light REE (Lu_N/Sm_N = 2.56–315.92; av. 67.68), a lower average \sum REE of 1248 ppm, Th/U ratios usually <1.0, and Th and U concentrations as low as 31 and 41 ppm, respectively. A few crystals provided apparent Jurassic dates (~160-200 Ma) but had geochemistry and REE patterns similar to the prevalent Cretaceous zircons. We attribute such this occasional bias in apparent dates to the surface ablation method we employed (for instance, some ²⁰⁶Pb/²³⁸U dates had imprecisions approaching 15% at 2σ level), and the likely influence of uncorrected common Pb on crystal surfaces. The reproducibility of the REE and other trace element concentrations in these phenocrysts is evidence for the geochemical integrity of the residual zircon crystals after chemical separation. Overall, we recommend a rapid combined geochemical and age screening technique by LA-ICPMS for investigative purposes as a powerful complementary routine to discriminate different zircon populations and other refractory minerals in the chemical dissolution residues.

Six zircon crystals selected from the chemical dissolution residue of FC1-A yielded concordant (within decay constant uncertainty) and equivalent U—Pb isotope ratios (Table 6) with calculated weighted mean $^{206}\text{Pb}/^{238}\text{U}$ and $^{207}\text{Pb}/^{206}\text{Pb}$ dates of 1095.86 ± 0.24 Ma and 1098.24 ± 0.33 Ma, respectively (Fig. 6). These results are statistically identical to those reported by Swanson-Hysell et al. (2021) for crystals extracted by conventional physical separation from the same sample $(^{206}\text{Pb}/^{238}\text{U}$ and $^{207}\text{Pb}/^{206}\text{Pb}$ dates of 1095.81 ± 0.16 Ma and 1098.21 ± 0.25 Ma, respectively). These results attest to the fact that the proposed chemical dissolution method does not introduce analytical bias or laboratory-induced open-system behavior in the residual crystal isotopic systematics.

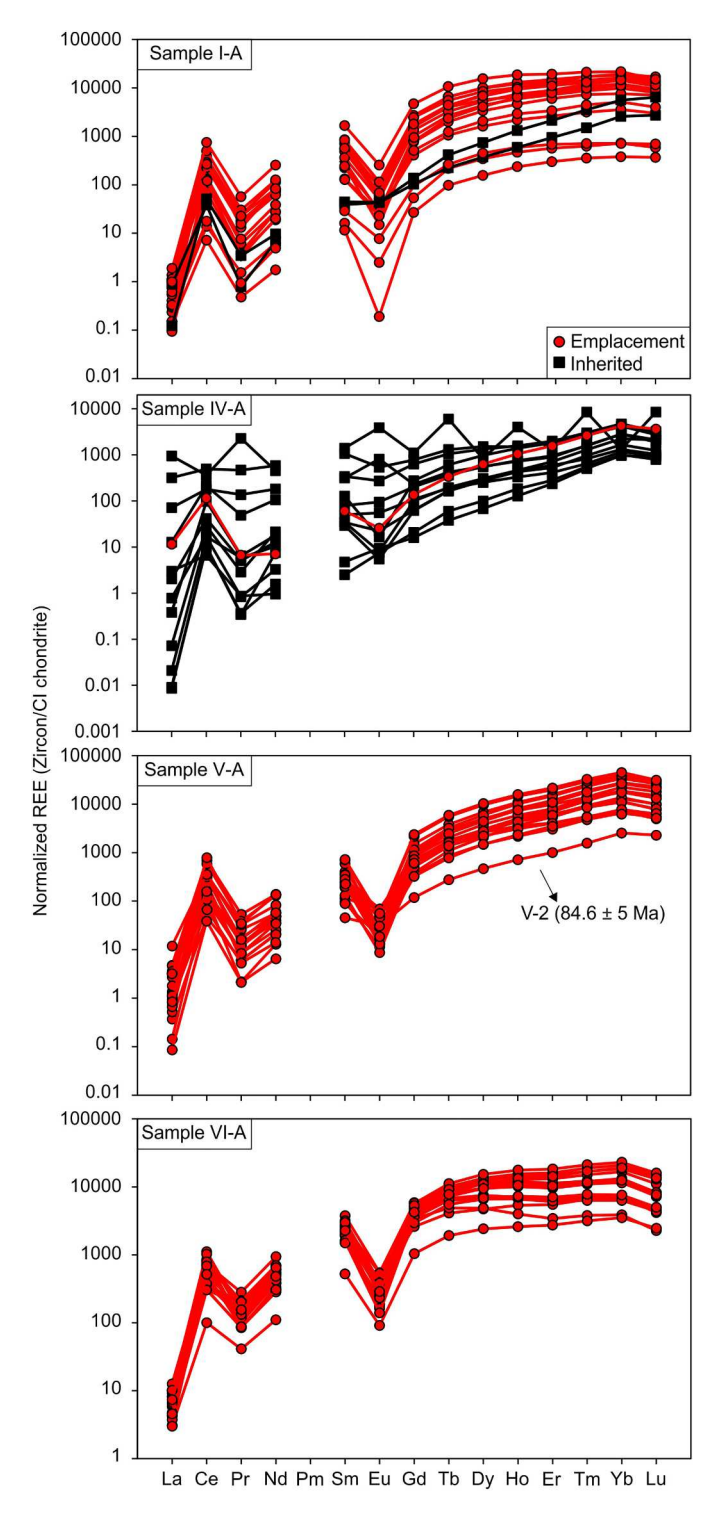


Fig. 5. Multi element REE diagram normalized to CI-chondrite (Sun and McDonough, 1989) for zircon crystals extracted by the chemical dissolution method. Red – emplacement-related zircons. Black – inherited zircons. (For interpretation of the references to color in this figure legend, the reader is referred to the web version of this article.)

4. Discussion

4.1. Optimal dissolution routine

The optimal dissolution routine was designed based on the best sample aliquot of the first experimental phase (beaker 13; Table 3),

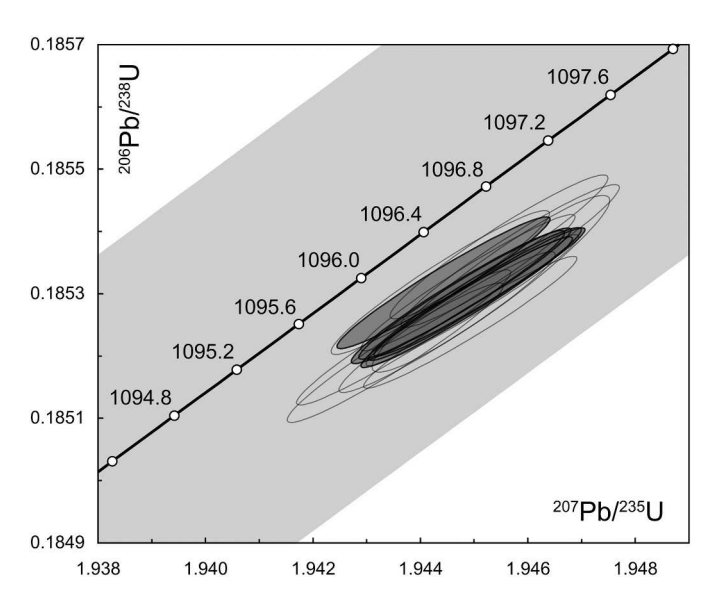


Fig. 6. Results from FC1-A, comparing the new results (dark gray) to those published in Swanson-Hysell et al., 2021 (open). Note that no apparent age bias is introduced by preparing samples using the bulk chemical dissolution method for zircon concentration. Light gray is the concordia decay constant uncertainty band, all errors are 2σ .

Table 5
Zircon identity from LA-ICPMS analysis.

Sample	Magnetic fraction (g)	Dissolved	# of zircon	# zircon
	(% initial aliquot)	sample (g)	crystals	crystals / g
ST05- 03-B	6.9 (1.1%)	6.06	11	1.8
I-B	158.9 (17.0%)	8.41	0	0.0
VI-B	173.0 (37.9%)	8.13	30	3.7

while also using the second experimental phase to evaluate the main parameter to be considered prior to the dissolution of a sample, i.e., the sample-to-acid ratio. This ratio must be decided on the first dissolution step, latter maintaining the acid volume to all other steps. Mafic minerals are more difficult to digest, and as a result greater modal proportions of pyroxenes, olivine and Fe-Ti-oxides require a lower sample-to-reagent ratio. As a guideline, tholeitic basalts can be dissolved at a proportion of approximately 0.10 g of rock to 1 ml of acid (g/ml), olivine-basalts at \sim 0.075 g/ml, and anorthosites/leucogabbros can be treated with up to 0.20 g/ml.

By way of illustration (schematically represented in Fig. 4), to dissolve 5 g of a dolerite one must use 20 ml of acid in each dissolution step – e.g., 20 ml of aqua regia in step one (24 h), 20 ml of hydrofluoric acid in step two (24 h), followed by another dissolution step of 20 ml of aqua regia (4 h), and a last step of 20 ml of hydrochloric acid (see sample ST05–03-A, beaker 2; Table 3). Initially (on the first two experimental phases shown on Table 3), the last HCl step was done immersed on an ultrasonic bath, but further evaluations showed that using the ultrasonic cleaner could break up the chemically attacked zircon crystals. Therefore, the last step was replaced by 2 h on concentrated HCl on a hot plate (as illustrated on Fig. 4). Rinsing with Milli-Q water must be done between each acid step to fully remove the dissolved material in solution and to clean the sample for the next acid attack, ensuring that undesirable reactions between the acids do not occur.

Additionally, if the zircon picking procedure ends up being hindered by abundant 'phantom' silicate crystals, we suggest repeating the last dissolution step (2 h on HCl). Usually, one repetition will be enough to dissolve the remaining non-zircon material (except rutile and Mgspinels) since the reason for them surviving thus far is the saturation

Chemical Geology 597 (2022)

Table 6
Zircon CA-IDTIMS results.

Sample	Compositional Parameters							Radiogenic Isotope Ratios									Isotopic Ages					
	Th	²⁰⁶ Pb*	mol %	Pb*	Pb_c	²⁰⁶ Pb ²⁰⁴ Pb	²⁰⁸ Pb	²⁰⁷ Pb ²⁰⁶ Pb	% err	²⁰⁷ Pb	% err	²⁰⁶ Pb ²³⁸ U	% err	corr.	²⁰⁷ Pb		²⁰⁷ Pb		²⁰⁶ Pb			
	U	$x10^{-13}$ mol	²⁰⁶ Pb*	Pbc	(pg)					²³⁵ U				coef.	²⁰⁶ Pb	±	²³⁵ U	±	²³⁸ U	±		
(a)	(b) (c)	(c)	(c)	(c)	(d)	(e)	(e)	(f)	(e)	(f)	(e)	(f)		(g)	(f)	(g)	(f)	(g)	(f)			
FC1-A																						
z1	0.646	26.8044	99.98%	1725	0.41	98,467	0.196	0.07613	0.040	1.945080	0.083	0.185302	0.045	0.974	1098.5	0.8	1096.75	0.56	1095.87	0.45		
z2	0.595	32.1998	99.99%	3006	0.28	173,661	0.180	0.07613	0.040	1.944997	0.084	0.185299	0.047	0.969	1098.4	0.8	1096.72	0.56	1095.86	0.47		
z3	0.589	36.9651	100.00%	6591	0.15	381,259	0.179	0.07612	0.040	1.944806	0.083	0.185299	0.046	0.969	1098.2	0.8	1096.66	0.56	1095.86	0.47		
z4	0.591	34.3365	99.99%	6194	0.14	358,137	0.179	0.07613	0.040	1.944840	0.083	0.185285	0.046	0.972	1098.4	0.8	1096.67	0.56	1095.78	0.46		
z5	0.591	22.2274	99.99%	2677	0.22	154,783	0.179	0.07610	0.041	1.944406	0.084	0.185317	0.046	0.967	1097.6	0.8	1096.52	0.56	1095.95	0.47		
z6	0.526	22.1282	99.99%	2200	0.26	129,305	0.159	0.07612	0.040	1.944679	0.084	0.185294	0.047	0.967	1098.2	0.8	1096.61	0.56	1095.83	0.47		
		$^{1}b/^{238}U \text{ age} = 10$ $^{1}b/^{206}Pb \text{ age} = 1$				(2 s); MSWD	= 0.06 (n = 0.06)															

- (a) z1, z2 etc. are labels for single zircon grains or fragments annealed and bulk chemically isolated, and then chemically abraded at 190 °C for 12 h after Mattinson (2005); bold indicates results used in weighted mean calculations.
- (b) Model Th/U ratio iteratively calculated from the radiogenic 208Pb/206Pb ratio and 206Pb/238 U age.
- (c) Pb* and Pbc represent radiogenic and common Pb, respectively; mol % ²⁰⁶Pb* with respect to radiogenic, blank and initial common Pb.
- (d) Measured ratio corrected for spike and fractionation only. Fractionation estimated from the ET535 double spike U ratio, and ET2535 double spike Pb analyses measured in the same interval.
- (e) Corrected for fractionation, spike, and common Pb; all common Pb was assumed to be procedural blank: $206Pb/204Pb = 18.042 \pm 0.61\%$; $207Pb/204Pb = 15.537 \pm 0.52\%$; $208Pb/204Pb = 37.686 \pm 0.63\%$ (all uncertainties 1-sigma).
- (f) Errors are 2-sigma, propagated using the algorithms of Schmitz and Schoene (2007).
- (g) Calculations are based on the decay constants of Jaffey et al. (1971) and 238 U/235 U = 137.88 (Steiger and Jäger, 1977). 206Pb/238 U and 207Pb/206Pb ages corrected for initial disequilibrium in 230Th/238 U using Th/U(magma) = 2.8 ± 0.05 (1 s).
- (h) Age uncertainties reported at the 95% confidence interval, as \pm analytical (+tracer) [+decay constant]; MSWD = mean squared weighted deviation. The 95% confidence interval is computed as the internal standard deviation multiplied by the Student's t-distribution multiplier for a two-tailed 95% critical interval and n-1 degrees of freedom for MSWD <1+2*sqrt[2/(n-1)] (Wendt and Carl, 1991), or expanded via multiplication by the sqrt(MSWD) when the MSWD $\ge 1+2*$ sqrt[2/(n-1)], in order to accommodate unknown sources of overdispersion.

of the reagent solution, not the refractory nature of those crystals.

A.L. Oliveira et al.

4.2. Comparing the conventional and chemical separation methods

The conventional separation method consists of treating the T1 aliquot by two main aspects: a (1) magnetic (hand magnet and Frantz) and a (2) density (heavy liquid) separation. These two separations have a consistent distinction when applied to zircon-rich coarse-grained (e.g., ST05-03 leucogabbro) or to fine- to medium-grained (e.g., EQUAMP diabase) rocks. From all B/T1 fractions treated by (1), the nonmagnetic aliquots obtained for the (EQUAMP) basaltic samples varied from 2.3% to 1.35% of the initial processed mass, while the same aliquot of the ST05-03 leucogabbro represented a cut of 57% (Table 2). Additionally, separation (2) fractionates fine mafic samples even more, where zircons crystallized and occluded by silicate minerals (see black circle Fig. 2D) are potentially lost to flotation. For instance, sample I-B had only 0.01 g of final mineral aliquot compared to 6.31 g from ST05-03-B. Thus, from a direct assessment of the final mineral yield obtained for sample I-B, we could see that up to 99.99% of a fine-grained rock might be separated into aliquots that will not be checked for zircon, where the losses are derived mainly from separation (1). A similar progressive loss of baddelevite crystals during conventional magnetic and heavy liquid separations was described by Söderlund and Johansson (2002).

To test the effects of physical processing and assess whether and where small zircon crystals were getting lost during separation (1), we dissolved magnetic fractions from three samples (Table 5). In sample ST05-03-B only the ferromagnetic (hand magnet) aliquot was dissolved, while for samples I—B and VI-B both ferromagnetic and paramagnetic (hand magnet and Frantz) aliquots were proportionally reintegrated (Table 2) prior to dissolution. In total, 11 zircon crystals were found in 6.06 g dissolution of ST05-03-B_{mag}, although no zircon crystals were found in 8.41 g of sample I-B_{mag} and 30 zircon crystals were recovered from dissolving 8.13 g of sample VI-B_{mag}. The recovery of zircon from the magnetic fractions (Table 5) of samples VI-B_{mag} and ST05-03-B_{mag} show that the magnetic separation can influence the effectiveness of the conventional method for mafic rocks by triggering a loss of zircon crystals adhering to or encapsulated within ferromagnetic minerals. Furthermore, separation (2) might also be a potential process where zircon is lost, since we were able to see a zircon crystal occluded on a silicate (or phantom silicate) during the bulk dissolution of sample VI-B (Fig. 2D).

In contrast to the conventional separation, the bulk chemical dissolution technique is a process by which a sample is physically segregated only once, by density and size at the water table. Therefore, the sampled used on the bulk chemical dissolution technique represents an average portion of 22% of the initial whole rock sample (Table 2). Only one container is used immediately after water table separation minimizing potential losses and cross-contamination due to transfer between containers. Also, the standard density and magnetic separation techniques (from the conventional method) rely upon complete disaggregation into monomineralic sand to silt-sized grains to optimize mineral segregation, while chemical dissolution is insensitive to crystal aggregation.

Overall, there is a 15 to 1000-fold increase in the zircon yield using the chemical dissolution method in comparison to the conventional physical treatment (Tables 4). Sample VI-B is a good example of how such physical treatments might impact the zircon recovery on these types of rocks since only 5 crystals were handpicked from the final concentrate of 175.5 g of sample from the water table, less than the 30 crystals concentrated from the chemical dissolution of just 8.13 g of its magnetic (i.e., VI-B_{mag}) aliquots (Table 5), and the 451 crystals recovered by chemical dissolution of 12.22 g of water table concentrate (i.e. VI-A, Table 4). In a more profound example, 164.3 g of sample I-B water table concentrate yielded no zircon by the conventional method (Table 4), even though we were able to recover 53 crystals from 112.4 g of water concentrate using the chemical dissolution method.

5. Conclusion

The chemical dissolution method is efficient for concentrating zircon crystals for U—Pb geochronology from a range of mafic rocks containing minute quantities of zircon. The magnetic and density concentration by the conventional separation routine can lead to loss of zircon crystals associated with ferro- and paramagnetic minerals. To promote efficient dissolution, samples should be ground to $<\!500~\mu m$, and a dense mineral fraction may be concentrated by water table methods, with no further magnetic or heavy liquid separations required. Samples must be thermally annealed prior to chemical processing in order to retain closed-system behavior in crystalline zircon during dissolution of the bulk matrix. The dissolution routine that works most efficiently for mafic rocks consists of sequential treatments by aqua regia, hydrofluoric, and hydrochloric acids on a hot plate, in a proportion of 10 ml of acid per gram of sample for each dissolution step. In an effective dissolution, the residual minerals are restricted to zircon, rutile, and magnesian spinels.

Noteworthy, the modal quantity of oxides is a determining factor to the chemical dissolution method. The presence of large amounts of non-silicate minerals tend to saturate the acid solutions (mainly the aqua regia steps) and hinder the overall dissolution efficiency. The same is not true for silicate-rich rocks because the HF is highly effective in breaking the silica bonds. This difference is observable in the leucogabbro and anorthosite samples (as well as the basaltic andesite sample VI), where the successful sample-to-acid ratio can be up to two times larger than for diabase. Therefore, even though mafic rocks benefit the most from this method, more intermediate to felsic rocks, for example aluminosilicate-rich metamorphic rocks, might also be suited to this method.

By using the chemical dissolution method, zircon can be readily recovered from grams of rock processed and efficiencies can be up to a hundred times greater when compared to the conventional/physical separation method. Such advantage is related to the lack of repetitive physical segregation, enabling the preservation (and concentration) of small zircon crystals that can be lost during physical separation when occluded by more magnetic or less dense grains. Of course, the high-temperature annealing of the bulk sample heavy obviates the use of the separated zircon for (U + Th + Sm)-He and fission track thermochronology. Also, our aggressive chemical dissolution procedure also appears to dissolve baddeleyite, although recent experiments by Guo et al. (2022) indicate that chemical dissolution can also be modulated to successfully separate this mineral.

The ability to date fine-grained mafic rocks (basaltic flows, diabase dikes and sills) is of great interest to critical geologic problems like determining the timing of catastrophic events (in particular mass extinction events), continental break up, and the duration and tempo of large igneous events. By treating tholeiitic dikes and cumulate maficultramafic rocks by the chemical dissolution method we were able to obtain zircon crystals from all samples tested, suggesting that this method can promote U—Pb zircon dating for a variety of different tectonomagmatic environments that require mafic rock geochronology.

Declaration of Competing Interest

The authors declare that they have no known competing financial interests or personal relationships that could have appeared to influence the work reported in this paper.

Acknowledgements

ALO acknowledges Brazilian agencies Coordination of Superior Level Staff Improvement (CAPES) for financial support during a one-year research scholarship at Boise State, and the National Council for Scientific and Technological Development (CNPq) for his PhD scholarship. MDS acknowledges funding for the analytical infrastructure of the Boise State Isotope Geology Laboratory through NSF Major Research Instrumentation grants EAR-0521221, EAR-1337887, and EAR-1920336, and

NSF EAR Instrumentation and Facilities Program grant EAR-0824974. CJW acknowledges financial support through NSF EAR Instrumentation and Facilities Program grant EAR-1735889. MHBMH is thankful to the CNPq for the research fellowship no. 303201/2019-3. Two anonymous reviews and the editorial handling by Dr. Balz Kamber greatly improved the final presentation of the manuscript.

Appendix A. Supplementary data

Supplementary data to this article can be found online at $\frac{https:}{doi.}$ org/10.1016/j.chemgeo.2022.120817.

References

- Bacon, C.R., 1989. Crystallization of accessory phases in magmas by local saturation. Geochim. Cosmochim. Acta 53, 1055–1066. https://doi.org/10.1016/0016-7037 (80)90210-X
- Bea, F., Montero, P., Palma, J.F.M., 2018. Experimental evidence for the preservation of U-Pb isotope ratios in mantle-recycled crustal zircon grains. Sci. Rep. 1–10 https://doi.org/10.1038/s41598-018-30934-4.
- Begemann, F., Ludwig, K.R., Lugmair, G.W., Min, K., Nyquist, L.E., Patchett, P.J., Renne, P.R., Shih, C.Y., Villa, I.M., Walker, R.J., 2001. Call for an improved set of decay constants for geochronological use. Geochim. Cosmochim. Acta 65, 111–121. https://doi.org/10.1016/S0016-7037(00)00512-3.
- Bleeker, W., Ernst, R., 2006. Short-lived mantle generated magmatic events and their dyke swarms: the key unlocking Earth's paleogeographic record back to 2.6 Ga. In: Hanski, E., Mertanen, S., Rämö, T., Vuollo, J. (Eds.), Dyke Swarms -Time Markers of Crustal Evolution. A.A. Balkema Publishers, Rotterdam, pp. 1–24. https://doi.org/10.1201/NOE0415398992.ch1\r10.1201/NOE0415398992.ch1
- Boehnke, P., Watson, E.B., Trail, D., Harrison, T.M., Schmitt, A.K., 2013. Zircon saturation re-revisited. Chem. Geol. 351, 324–334. https://doi.org/10.1016/j. chem.eo. 2013.05.028
- Chamberlain, K.R., Schmitt, A.K., Swapp, S.M., Harrison, T.M., Swoboda-Colberg, N., Bleeker, W., Peterson, T.D., Jefferson, C.W., Khudoley, A.K., 2010. In situ U-Pb SIMS (IN-SIMS) micro-baddeleyite dating of mafic rocks: method with examples. Precambrian Res. 183, 379–387. https://doi.org/10.1016/j.precamres.2010.05.004.
- Davies, J.H.F.L., Marzoli, A., Bertrand, H., Youbi, N., Ernesto, M., Schaltegger, U., 2017. End-Triassic mass extinction started by intrusive CAMP activity. Nat. Commun. 8, 1–8. https://doi.org/10.1038/ncomms15596.
- Davis, W.J., Davis, D.W., 2010. Alpha recoil loss from baddeleyite evaluated by depth profiling and numerical modelling: implications for U-Pb ages. In: Goldschmidt Conference Abstracts (P. A213).
- Davis, D.W., Krogh, T.E., 2001. Preferential dissolution of 234U and radiogenic Pb from α -recoil-damaged lattice sites in zircon: implications for thermal histories and Pb isotopic fractionation in the near surface environment. Chem. Geol. 172, 41–58. https://doi.org/10.1016/S0009-2541(00)00235-7.
- Davis, D.W., Williams, I.S., Krogh, T.E., 2003. Historical development of zircon geochronology. Rev. Mineral. Geochem. 53, 145–181.
- Doe, B.R., Newell, M.F., 1965. Isotopic composition of uranium in zircon. Am. Mineral. 50, 613–618.
- Ernst, R.E., Bleeker, W., Söderlund, U., Kerr, A.C., 2013. Large Igneous Provinces and supercontinents: toward completing the plate tectonic revolution. Lithos 174, 1–14. https://doi.org/10.1016/j.lithos.2013.02.017.
- Fourny, A., Weis, D., Scoates, J.S., 2016. Comprehensive Pb-Sr-Nd-Hf isotopic, trace element, and mineralogical characterization of mafic to ultramafic rock reference materials. Geochem. Geophys. Geosyst. 17, 739–773. https://doi.org/10.1002/ 2015GC006181.
- Guo, Q., Li, Q.L., Chu, Z.Y., Ling, X.X., Guo, S., Xue, Ding-Shuai, Yin, Qing-Zhu, 2022. An acid-based method for highly effective baddeleyite separation from gram-sized mafic rocks. Anal. Chem. https://doi.org/10.1021/acsomega.1c06264.
- Harrison, T.M., Watson, E.B., Aikman, A.B., 2007. Temperature spectra of zircon crystallization in plutonic rocks. Geology 35, 635–638. https://doi.org/10.1130/ G23505A.1.
- Heaman, L.M., 2009. The application of U-Pb geochronology to mafic, ultramafic and alkaline rocks: an evaluation of three mineral standards. Chem. Geol. 261, 43–52. https://doi.org/10.1016/j.chemgeo.2008.10.021.
- Heaman, L.M., LeCheminant, A.N., 2001. Anomalous U-Pb systematics in mantle-derived baddeleyite xenocrysts from Île Bizard: evidence for high temperature radon diffusion? Chem. Geol. 172, 77–93. https://doi.org/10.1016/S0009-2541(00) 00237-0.
- Heaman, L.M., LeCheminant, A.N., Rainbird, R.H., 1992. Nature and timing of Franklin igneous events, Canada: Implications for a Late Proterozoic mantle plume and the break-up of Laurentia. Earth Planet. Sci. Lett. 109, 117–131. https://doi.org/ 10.1016/0012-821X(92)90078-A.
- Heimdal, T.H., Svensen, H.H., Ramezani, J., Iyer, K., Pereira, E., Rodrigues, R., Jones, M. T., Callegaro, S., 2018. Large-scale sill emplacement in Brazil as a trigger for the end-triassic crisis. Sci. Rep. 8, 1–12. https://doi.org/10.1038/s41598-017-18629-8.
- Hollanda, M.H.B.M., Archanjo, C.J., Macedo Filho, A.A., Fossen, H., Ernst, R.E., de Castro, D.L., Melo, A.C., Oliveira, A.L., 2019. The Mesozoic Equatorial Atlantic Magmatic Province (EQUAMP): a new large Igneous Province in South America. In: Srivastava, R., Ernst, R.E., Peng (Eds.), Dyke Swarms of the World: A Modern

- Perspective. Springer Singapore, pp. 87–110. https://doi.org/10.1007/978-981-13-
- Ibañez-Mejia, M., Tissot, F.L.H., 2019. Extreme Zr stable isotope fractionation during magmatic fractional crystallization. Sci. Adv. 5, 12. https://doi.org/10.1126/sciadv. 2288648
- Ireland, T.R., Williams, I.S., 2003. Considerations in zircon geochronology by SIMS. Rev. Miner. Geochem. 53, 215–241. https://doi.org/10.2113/0530215.
- Isakson, V.H., Schmitz, M.D., Dehler, C.M., Macdonald, F.A., Yonkee, W.A., 2022.
 A robust age model for the Cryogenian Pocatello Formation of southeastern Idaho (northwestern USA) from tandem in situ and isotope dilution U-Pb dating of volcanic tuffs and epiclastic detrital zircons. Geosphere 1–25. https://doi.org/10.1130/GFS0.2437.1
- Jaffey, A.H., Flynn, K.F., Glendenin, L.E., Bentley, W.C., Essling, A.M., 1971. Precision measurement of half-lives and specific activities of 235U and 238U. Phys. Rev. C 4, 1889–1906. https://doi.org/10.1103/PhysRevC.4.1889.
- Krogh, T.E., 1973. A low-contamination method for hydrothermal decomposition of zircon and extraction of U and Pb for isotopic age determinations. Geochim. Cosmochim. Acta 37, 485–494. https://doi.org/10.1016/0016-7037(73)90213-5.
- Krogh, T.E., Corfu, F., Davis, D., Dunning, G., Heaman, L., Kamo, S., Machado, N., Greenough, J., Nakamura, E., 1987. Precise U–Pb isotopic ages of diabase dykes. In: Halls, H., Fahrig, W. (Eds.), Mafic Dyke Swarms. Geological Association of Canada, Special Paper, 34, pp. 147–152.
- Larsen Jr., E.S., Keevil, N.B., Harrison, H.C., 1952. Method for determining the age of igneous rocks using the accessory minerals. Geol. Soc. Am. Bull. 63, 1045–1052. https://doi.org/10.1130/0016-7606(1952)63[1045:MFDTAO]2.0.CO;2.
- Lawley, C., Selby, D., 2012. Re-Os geochronology of quartz-enclosed ultrafine molybdenite: implications for ore geochronology. Econ. Geol. 107, 1499–1505. https://doi.org/10.2113/econgeo.107.7.1499.
- LeCheminant, A.N., Heaman, L.M., 1989. Mackenzie igneous events, Canada: middle Proterozoic hotspot magmatism associated with ocean opening. Earth Planet. Sci. Lett. 96, 38–48. https://doi.org/10.1016/0012-821X(89)90122-2.
- Lee, C.T.A., Bachmann, O., 2014. How important is the role of crystal fractionation in making intermediate magmas? Insights from Zr and P systematics. Earth Planet. Sci. Lett. 393, 266–274. https://doi.org/10.1016/j.epsl.2014.02.044.
- Li, Q.L., Li, X.H., Liu, Y., Tang, G.Q., Yang, J.H., Zhu, W.G., 2010. Precise U-Pb and Pb-Pb dating of Phanerozoic baddeleyite by SIMS with oxygen flooding technique. J. Anal. At. Spectrom. 25, 1107–1113. https://doi.org/10.1039/b923444f.
- Macdonald, F.A., Schmitz, M.D., Strauss, J.V., Halverson, G.P., Gibson, T.M., Eyster, A., Cox, G., Mamrol, P., Crowley, J.L., 2018. Cryogenian of Yukon. Precambrian Res. 319, 114–143. https://doi.org/10.1016/j.precamres.2017.08.015.
- Macêdo Filho, A.A., Hollanda, M.H.B.M., 2022. Petrogenesis of Mesozoic giant dike swarms and geodynamical insights about Gough flavors near the Equatorial Atlantic margin (NE South America). Lithos 413, 106611.
- Mattinson, J.M., 1994. A study of complex discordance in zircons using step-wise dissolution techniques. Contrib. Mineral. Petrol. 116, 117–129. https://doi.org/ 10.1007/BF00310694.
- Mattinson, J.M., 2005. Zircon U-Pb chemical abrasion ("CA-TIMS") method: combined annealing and multi-step partial dissolution analysis for improved precision and accuracy of zircon ages. Chem. Geol. 220, 47–66. https://doi.org/10.1016/j. chemica. 2005.03.011
- Mattinson, J.M., 2011. Extending the krogh legacy: development of the CA-TIMS method for zircon U-Pb geochronology. Can. J. Earth Sci. 48, 95–105. https://doi.org/ 10.1139/F10-023
- Miller, J.D., Weiblen, P.W., 1990. Anorthositic rocks of the Duluth complex: examples of rocks formed from plagioclase crystal mush. J. Petrol. 31, 295–339. https://doi.org/ 10.1093/petrology/31.2.295.
- Neuerburg, G.J., 1961. A method of mineral separation using hydrofluoric acid. Am. Mineral. 46, 1498–1501.
- Nilsson, M.K.M., Söderlund, U., Ernst, R.E., Hamilton, M.A., Scherstén, A., Armitage, P.E. B., 2010. Precise U-Pb baddeleyite ages of mafic dykes and intrusions in southern West Greenland and implications for a possible reconstruction with the Superior craton. Precambrian Res. 183, 399–415. https://doi.org/10.1016/j. precamres.2010.07.010.
- Oliveira, A.L., Hollanda, M.H.B.M., Siqueira, R., Macêdo Filho, A.A., 2021. Using a 'speedy' unspiked K-Ar methodology to investigate age patterns in giant mafic dike swarms. Geol. Soc. London Spec. Publ. 518 https://doi.org/10.1144/sp518-2020-250. SP518-2020-250.
- Paces, J.B., Miller, J.D., 1993. Precise U-Pb ages of Duluth Complex and related mafic intrusions, northeastern Minnesota: geochronological insights to physical, petrogenetic, paleomagnetic, and tectonomagmatic processes associated with the 1.1 Ga Midcontinent Rift system. J. Geophys. Res. 98 https://doi.org/10.1029/ 93jb01159.
- Pohlner, J.E., Schmitt, A.K., Chamberlain, K.R., Davies, J.H.F.L., Hildenbrand, A., Austermann, G., 2020. Multimethod U-Pb baddeleyite dating: insights from the Spread Eagle Intrusive Complex and Cape St. Mary's sills, Newfoundland, Canada. Geochronology 2, 187–208. https://doi.org/10.5194/gchron-2-187-2020.
- Rioux, M., Bowring, S., Dudás, F., Hanson, R., 2010. Characterizing the U-Pb systematics of baddeleyite through chemical abrasion: application of multi-step digestion methods to baddeleyite geochronology. Contrib. Mineral. Petrol. 160, 777–801. https://doi.org/10.1007/s00410-010-0507-1.
- Schaltegger, U., Davies, J.H.F.L., 2017. Petrochronology of zircon and baddeleyite in igneous rocks: reconstructing magmatic processes at high temporal resolution. Rev. Mineral. Geochem. 83, 297–328. https://doi.org/10.2138/rmg.2017.83.10.
- Schaltegger, U., Schmitt, A.K., Horstwood, M.S.A., 2015. U-Th-Pb zircon geochronology by ID-TIMS, SIMS, and laser ablation ICP-MS: Recipes, interpretations, and

- opportunities. Chem. Geol. 402, 89–110. https://doi.org/10.1016/j.chemgeo.2015.02.028.
- Schmitz, M.D., Schoene, B., 2007. Derivation of isotope ratios, errors, and error correlations for U-Pb geochronology using 205Pb-235U-(233U)-spiked isotope dilution thermal ionization mass spectrometric data. Geochem. Geophys. Geosyst. 8, 1–20. https://doi.org/10.1029/2006GC001492.
- Schoene, B., Eddy, M.P., Samperton, K.M., Keller, C.B., Keller, G., Adatte, T., Khadri, S.F. R., 2019. U-Pb constraints on pulsed eruption of the Deccan Traps across the end-Cretaceous mass extinction. Science (80-.) 363, 862–866. https://doi.org/10.1126/science.aau2422.
- Silver, L., Deutsch, S., 1963. Uranium-lead isotopic variations in zircons: a case study. J. Geol. 71, 721–758.
- Söderlund, U., Johansson, L., 2002. A simple way to extract baddeleyite (ZrO2). Geochem. Geophys. Geosyst. 3 https://doi.org/10.1029/2001gc000212, 1 of 7–7 7.
- Steiger, R.H., Jäger, E., 1977. Subcommission on geochronology: convention on the use of decay constants in geo-and cosmochronology. Earth Planet. Sci. Lett. 36, 359–362.
- Stevens, N.J., Seiffert, E.R., O'Connor, P.M., Roberts, E.M., Schmitz, M.D., Krause, C., Gorscak, E., Ngasala, S., Hieronymus, T.L., Temu, J., 2013. Palaeontological evidence for an Oligocene divergence between Old World monkeys and apes. Nature. https://doi.org/10.1038/nature12161.
- Stewart, R.A., 1986. Routine heavy mineral analysis using a concentrating table.

 J. Sediment. Res. 56, 555–556. https://doi.org/10.1306/212F89B8-2B24-11D7-8648000102C1865D
- Sun, S.S., McDonough, W.F., 1989. Chemical and isotopic systematics of oceanic basalts: Implications for mantle composition and processes. Geol. Soc. Spec. Publ. 42, 313–345. https://doi.org/10.1144/GSL.SP.1989.042.01.19.
- Swanson-Hysell, N.L., Hoaglund, S.A., Crowley, J.L., Schmitz, M.D., Zhang, Y., Miller, J. D., 2021. Rapid emplacement of massive Duluth Complex intrusions within the North American Midcontinent Rift. Geology 49, 185–189. https://doi.org/10.1130/G47873.1.
- Teixeira, W., Hamilton, M.A., Lima, G.A., Ruiz, A.S., Matos, R., Ernst, R.E., 2015. Precise ID-TIMS U-Pb baddeleyite ages (1110-1112Ma) for the Rincón del Tigre-Huanchaca large igneous province (LIP) of the Amazonian Craton: Implications for the Rodinia

- supercontinent. Precambrian Res. 265, 273–285. https://doi.org/10.1016/j.precamres.2014.07.006.
- Teixeira, W., Hamilton, M.A., Girardi, V.A.V., Faleiros, F.M., Ernst, R.E., 2019. U-Pb baddeleyite ages of key dyke swarms in the Amazonian Craton (Carajás/Rio Maria and Rio Apa areas): tectonic implications for events at 1880, 1110 Ma, 535 Ma and 200 Ma. Precambrian Res. 329, 138–155. https://doi.org/10.1016/j.precamres.2018.02.008.
- Tilton, G.R., 1956. The interpretation of lead-age discrepancies by acid-washing experiments. Eos Trans. Am. Geophys. Union 37, 224–230. https://doi.org/10.1029/TR037i002p00224.
- Tilton, G.R., Davis, G.L., Wetherill, G.W., Aldrich, L.T., 1957. Isotopic ages of zircon from granites and pegmatites. Eos Trans. Am. Geophys. Union 38, 360–371. https://doi.org/10.1029/TR038i003p00360.
- Todt, W.A., and Büsch, W. 1981. U–Pb investigations on zircons from pre-Variscan gneisses I. A study from the Schwartz- wald, West Germany, Geochim. Cosmochim. Acta, 45, 1789–1801. doi:https://doi.org/10.1016/0016-7037(81) 00010-7
- Wall, C.J., Scoates, J.S., Weis, D., 2016. Zircon from the Anorthosite zone II of the Stillwater Complex as a U-Pb geochronological reference material for Archean rocks. Chem. Geol. 436, 54–71. https://doi.org/10.1016/j.chemgeo.2016.04.027.
- Wall, C.J., Scoates, J.S., Weis, D., Friedman, R.M., Amini, M., Meurer, W.P., 2018. The Stillwater Complex: integrating zircon geochronological and geochemical constraints on the age, emplacement history and crystallization of a large, opensystem layered intrusion. J. Petrol. 59, 153–190. https://doi.org/10.1093/ petrology/eng/024
- Watson, E.B., Harrison, T.M., 1983. Zircon saturation revisited: temperature and composition effects in a variety of crustal magma types. Earth Planet. Sci. Lett. 64, 295–304. https://doi.org/10.1016/0012-821X(83)90211-X.
- Wendt, I., Carl, C., 1991. The statistical distribution of the mean squared weighted deviation. Chem. Geo.: Isotope Geoscience Section 86, 275–285. https://doi.org/ 10.1016/0168-9622(91)90010-T.
- Wetherill, G.W., 1956. Discordant uranium-lead ages, I. Eos Trans. Am. Geophys. Union 37, 320–326. https://doi.org/10.1029/TR037i003p00320.